Mathematics

AIMS Mathematics, 10(9): 20346–20367.
DOI: 10.3934/math.2025909
Received: 06 July 2025
Revised: 21 August 2025
Accepted: 25 August 2025
Published: 05 September 2025

https://www.aimspress.com/journal/Math

Research article

Constructing a 5D Hamiltonian conservative hyperchaotic system with amplitude control, multistability, and wide constant range

Birong Xu[1,*] and Zhitao Xu[2]

[1] College of Mechanic and Electronic Engineering, Wuyi University, Wuyishan 354300, China
[2] Department of Computer Science and Engineering, Southern University of Science and Technology, Shenzhen 518055, China

*** Correspondence:** Email: xubirong1@163.com.

Abstract: This paper presents the construction of a 5D Euler equation using four sub-Euler equations with the coupling parameters and analyzes the conservation of Hamiltonian and Casimir energy. By breaking the conservation of Casimir energy, a 5D Hamiltonian conservative hyperchaotic system is developed. Phase diagrams, Lyapunov exponent spectra, and bifurcation diagrams are employed to investigate the nonlinear properties of the system. It is discovered that the system possesses dynamic characteristics such as amplitude control, multistability, transient quasi-period, and a wide constant range. The statistical properties of the pseudo-random sequences produced by the system are assessed via the National Institute of Standards and Technology (NIST). Lastly, the circuit simulation and STM32 platform are used to confirm the viability of the system.

Keywords: 5D Euler equations; Hamiltonian conservative hyperchaotic system; multistability; wide constant range; amplitude control
Mathematics Subject Classification: 34C28, 37D45

1. Introduction

In the realm of nonlinear dynamics, chaos theory has garnered extensive attention owing to its profound implications across diverse fields such as information security, biology, physics, and engineering [1–6]. Chaotic systems, which are distinguished by their sensitivity to initial conditions and complicated, unpredictable behavior, have been extensively explored for both theoretical and

practical applications. In Reference [7], a memristive mega-stable system was proposed, which can produce dissipative behavior and conservative behavior with the change of control parameter. Among chaotic systems, conservative chaotic systems (CCSs) represent a unique category. Unlike dissipative chaotic systems (DCSs) that exhibit attractors and dissipate energy over time, the CCSs conserve their phase volume and energy, making them particularly intriguing for applications where reconstruction of attractors is not feasible and higher security is desired.

There is growing interest in the creation of high-dimensional conservative chaotic systems. Hyperchaotic phenomena occur only in conservative chaotic systems of more than three dimensions, and high-dimensional systems may offer more complex dynamics and greater potential for applications such as random number generation, image encryption, and secure communication. However, designing such systems is challenging due to the stringent requirements for conserving the Hamiltonian while ensuring chaotic behavior. Traditional methods often rely on extending and coupling lower-dimensional systems, which can limit flexibility and complexity [8–10].

In recent years, several studies have proposed innovative approaches to construct high-dimensional conservative chaotic or hyperchaotic systems. For instance, Cang et al. presented two conservative chaotic systems and used the perpetual point theory to identify their conservativeness [11]. In Reference [12], a 5D conservative memristive hyperchaotic system was proposed by integrating a memristor into a 4D CCS. Qi et al. [13–15] extended the 3D rigid body Euler equations to higher dimensions and coupled sub-Euler equations to create chaos by breaking the Casimir energy conservation law. These works have laid the foundation for further exploration into the dynamics of high-dimensional conservative systems.

Furthermore, there are two types of conservative chaotic systems: Hamiltonian conservative chaotic systems (HCCSs) and non-Hamiltonian conservative chaotic systems (Non-HCCSs). The HCCS possesses Hamiltonian conservation and zero divergence, while the Non-HCCS simply has the Lyapunov zero-sum form. The requirements for building the HCCS are more stringent, and the trajectories of the HCCS are more stable, so it has important theoretical and practical significance for the construction and analysis of the HCCS. Qi built 4D Euler equations by combining two sub-Euler equations with two common axes, and then realized 4D HCCSs by breaking the conservation of Casimir energies [13]. In Reference [16], a class of 4D HCCSs was constructed by coupling four sub-Euler equations with four coupling parameters, and it was found that these HCCSs exhibited transient quasi-period and multistability. In order to further explore 5D HCCSs, Dong et al. extended the 3D Euler equation to 5D by coupling two sub-bodies with one common axis, and broke the conservation of Casimir energy to generate a category of 5D Hamiltonian conservative hyperchaotic systems [17]. Through combining two sub-Euler equations with a single axis, Huang et al. created 5D Hamiltonian conservative hyperchaotic systems with a broad parameter range [18–20]. Ning et al. devised a 5D Hamiltonian conservative hyperchaotic system and used it for image encryption; encryption evaluations revealed that the encryption method possessed strong security [21]. Despite these advances, the theoretical foundation for Hamiltonian conservative hyperchaotic systems remains insufficient. Furthermore, multistability and hidden dynamic behaviors are special nonlinear phenomena and have been recent research hotspots. Reference [22] presented that the generalized U-shaped nonlinear SRR model has multistability. Really, HCCSs also own multistability. Reference [23] proposed a hidden multiwing memristive neural network. Multistability is often related to hidden dynamic behaviors. There is a need for more methods to construct high-dimensional systems with rich dynamical behaviors, such as broad parameter ranges and multistability, which are crucial

for practical applications. This study presents a novel way to construct the matrix of 5D Euler equations. A 5D conservative hyperchaotic system is built on the basis of this matrix, which preserves the Hamiltonian while allowing for the introduction of irregular variations in the Casimir power. We analyze the dynamic characteristics of the conservative hyperchaotic systems by numerical simulations, and further validate their properties through circuit simulations and hardware experiments. Then, through comparative analysis, the superiority of the proposed system is highlighted.

The remainder of the structure is arranged in the following. The theoretical foundations of the rigid body Euler equation, Hamiltonian, and Casimir energy are introduced in Section 2. Section 3 presents the proposed construction method and verifies its effectiveness through the design of a 5D conservative hyperchaotic system. Section 4 provides a full dynamical study of the constructed systems, including equilibrium points, divergence, coexisting hyperchaotic orbits, bifurcation diagrams, and Lyapunov exponents. Section 5 discusses the NIST test results. The practical feasibility of this system is demonstrated in Section 6 through the use of STM32 hardware implementation and analog circuit simulations. Section 7 compares the proposed system with the existing conservative chaotic systems. The main conclusions and contributions of this work are finally summed up in Section 8.

2. Constructing 5D generalized Euler equations

Without external force, the 3D Euler equation describing the dynamics of a rigid body is written as

$$\begin{aligned} \dot{x}_1 &= (c_3 - c_2)x_2x_3, \\ \dot{x}_2 &= (c_1 - c_3)x_3x_1, \\ \dot{x}_3 &= (c_2 - c_1)x_1x_2, \end{aligned} \tag{1}$$

where x_i is the angular momentum, and c_i is the reciprocal of inertia. System (1) is a Hamiltonian system. The Euler equation is described as

$$\dot{\boldsymbol{x}} = J(\boldsymbol{x})\nabla H(\boldsymbol{x}), \tag{2}$$

where J(x) is

$$J(\boldsymbol{x}) = -J^T(\boldsymbol{x}) = \begin{bmatrix} 0 & -x_3 & x_2 \\ x_3 & 0 & -x_1 \\ -x_2 & x_1 & 0 \end{bmatrix}, \tag{3}$$

and H(x) is

$$H(\boldsymbol{x}) = \frac{1}{2}(c_1x_1^2 + c_2x_2^2 + c_3x_3^2). \tag{4}$$

The corresponding Casimir energy can be expressed as

$$C(\boldsymbol{x}) = \frac{1}{2}(x_1^2 + x_2^2 + x_3^2). \tag{5}$$

To construct 5D Euler equations, we employ the 3D Euler equation to generate sub-bodies of the 5D

system. We have eight types of sub-bodies, which are Sub-body$_{123}$, Sub-body$_{124}$, Sub-body$_{125}$, Sub-body$_{134}$, Sub-body$_{135}$, Sub-body$_{234}$, Sub-body$_{235}$, Sub-body$_{245}$, and Sub-body$_{345}$. By introducing four coupling parameters k_i (i=1,2,3,4), the construction matrix of Euler equation is yielded as

$$\begin{aligned} J(\boldsymbol{x}) &= k_1 J_{1245}(\boldsymbol{x}) + k_2 J_{245}(\boldsymbol{x}) + k_3 J_{345}(\boldsymbol{x}) + k_4 J_{234}(\boldsymbol{x}) \\ &= k_1 \begin{bmatrix} 0 & 0 & 0 & -x_5 & x_4 \\ 0 & 0 & 0 & 0 & 0 \\ 0 & 0 & 0 & 0 & 0 \\ x_5 & 0 & 0 & 0 & -x_1 \\ -x_4 & 0 & 0 & x_1 & 0 \end{bmatrix} + k_2 \begin{bmatrix} 0 & 0 & 0 & 0 & 0 \\ 0 & 0 & 0 & -x_5 & x_4 \\ 0 & 0 & 0 & 0 & 0 \\ 0 & x_5 & 0 & 0 & -x_2 \\ 0 & -x_4 & 0 & x_2 & 0 \end{bmatrix} \\ &+ k_3 \begin{bmatrix} 0 & 0 & 0 & 0 & 0 \\ 0 & 0 & 0 & 0 & 0 \\ 0 & 0 & 0 & -x_5 & x_4 \\ 0 & 0 & x_5 & 0 & -x_3 \\ 0 & 0 & -x_4 & x_3 & 0 \end{bmatrix} + k_4 \begin{bmatrix} 0 & 0 & 0 & 0 & 0 \\ 0 & 0 & -x_5 & 0 & x_3 \\ 0 & x_5 & 0 & 0 & -x_2 \\ 0 & 0 & 0 & 0 & 0 \\ 0 & -x_3 & x_2 & 0 & 0 \end{bmatrix} \\ &= \begin{bmatrix} 0 & 0 & 0 & -k_1 x_5 & k_1 x_4 \\ 0 & 0 & -k_4 x_5 & -k_2 x_5 & k_2 x_4 + k_4 x_3 \\ 0 & k_4 x_5 & 0 & -k_3 x_5 & k_3 x_4 - k_4 x_2 \\ k_1 x_5 & k_2 x_5 & k_3 x_5 & 0 & -k_1 x_1 - k_2 x_2 - k_3 x_3 \\ -k_1 x_4 & -k_2 x_4 - k_4 x_3 & -k_3 x_4 + k_4 x_2 & k_1 x_1 + k_2 x_2 + k_3 x_3 & 0 \end{bmatrix}. \end{aligned} \tag{6}$$

Subsequently, a 5D Euler equation in the Hamiltonian vector field is expressed as

$$\sum \dot{\boldsymbol{x}} = J(\boldsymbol{x}) \nabla H(\boldsymbol{x}). \tag{7}$$

The mathematical model of System (7) is expressed as

$$\begin{cases} \dot{x}_1 = (c_5 - c_4) k_1 x_4 x_5, \\ \dot{x}_2 = (c_5 - c_4) k_2 x_4 x_5 + (c_5 - c_3) k_4 x_3 x_5, \\ \dot{x}_3 = (c_5 - c_4) k_3 x_4 x_5 + (c_2 - c_5) k_4 x_2 x_5, \\ \dot{x}_4 = (c_1 - c_5) k_1 x_1 x_5 + (c_2 - c_5) k_2 x_2 x_5 + (c_3 - c_5) k_3 x_3 x_5, \\ \dot{x}_5 = (c_4 - c_1) k_1 x_1 x_4 + (c_4 - c_2) k_2 x_2 x_4 + (c_4 - c_3) k_3 x_3 x_4 + (c_3 - c_2) k_4 x_2 x_3. \end{cases} \tag{8}$$

The values of the parameters k_i reflect the strength of the interaction between the sub-rigid bodies. The associated sub-rigid body has no effect on the multi-rigid body if a given k_i equals zero. Furthermore, the direction of the relative motion and interaction between the sub-rigid entities is determined by the magnitude and sign (positive or negative) of k_i. The parameter c_i is the reciprocal of inertia. All parameter values must be non-zero; otherwise, the 5D Euler equations cannot be realized. The corresponding 5D Hamiltonian is

$$H(\boldsymbol{x}) = \frac{1}{2}(c_1 x_1^2 + c_2 x_2^2 + c_3 x_3^2 + c_4 x_4^2 + c_5 x_5^2). \tag{9}$$

Since the $J(\mathbf{x})$ is symplectic, there exists

$$\dot{H}(\boldsymbol{x}) = \nabla H(\boldsymbol{x})^T J(\boldsymbol{x}) \nabla H(\boldsymbol{x}) = 0. \tag{10}$$

In other words, these 5D generalized Euler equations have conservative Hamiltonian. For System (8), the Casimir energy is

$$C(\boldsymbol{x}) = \frac{1}{2}(x_1^2 + x_2^2 + x_3^2 + x_4^2 + x_5^2). \tag{11}$$

Herein, the Casimir power is employed to judge whether a system may produce chaos. The Casimir power is described as

$$\dot{C}(\boldsymbol{x}) = \nabla C(\boldsymbol{x})^T J(\boldsymbol{x}) \nabla H(\boldsymbol{x}) = 0. \tag{12}$$

Hence, the Hamiltonian and Casimir energy of the 5D generalized Euler equations are conservative.

3. 5D novel Hamiltonian conservative hyperchaotic systems

To generate a Hamiltonian conservative hyperchaotic system, the conservation of Casimir energy must be broken. By substituting a perturbation parameter d into the matrix J_{12} (**x**), the new matrix is yielded as

$$J^H(\boldsymbol{x}) = \begin{bmatrix} 0 & 0 & -d & -k_1x_5 & k_1x_4 \\ 0 & 0 & -k_4x_5 & -k_2x_5 & k_2x_4 + k_4x_3 \\ d & k_4x_5 & 0 & -k_3x_5 & k_3x_4 - k_4x_2 \\ k_1x_5 & k_2x_5 & k_3x_5 & 0 & -k_1x_1 - k_2x_2 - k_3x_3 \\ -k_1x_4 & -k_2x_4 - k_4x_3 & -k_3x_4 + k_4x_2 & k_1x_1 + k_2x_2 + k_3x_3 & 0 \end{bmatrix}. \tag{13}$$

In the Hamiltonian vector field, the 5D novel Hamiltonian conservative hyperchaotic system is written as

$$\sum \dot{\boldsymbol{x}} = J^H(\boldsymbol{x}) \nabla H(\boldsymbol{x}). \tag{14}$$

It should be noted that, except for the diagonal of matrix J^{H}(**x**) in Eq (13), the perturbation parameter d can be located at any position to break the conservation of Casimir. Different perturbation positions of d will generate different Hamiltonian conserved chaotic systems, and System (13) is one of them. By mathematical models, the Hamiltonian conservative hyperchaotic system is described as

$$\begin{cases} \dot{x}_1 = (c_5 - c_4)k_1x_4x_5 - dc_3x_3, \\ \dot{x}_2 = (c_5 - c_4)k_2x_4x_5 + (c_5 - c_3)k_4x_3x_5, \\ \dot{x}_3 = (c_5 - c_4)k_3x_4x_5 + (c_2 - c_5)k_4x_2x_5 + dc_1x_1, \\ \dot{x}_4 = (c_1 - c_5)k_1x_1x_5 + (c_2 - c_5)k_2x_2x_5 + (c_3 - c_5)k_3x_3x_5, \\ \dot{x}_5 = (c_4 - c_1)k_1x_1x_4 + (c_4 - c_2)k_2x_2x_4 + (c_4 - c_3)k_3x_3x_4 + (c_3 - c_2)k_4x_2x_3. \end{cases} \tag{15}$$

Since J^H(**x**) is symplectic, it is easy to prove

$$\dot{H}(\boldsymbol{x}) = \nabla H(\boldsymbol{x})^T J^H(\boldsymbol{x}) \nabla H(\boldsymbol{x}) = 0. \tag{16}$$

The 5D system conserves Hamiltonian. The Casimir power is described as

$$\dot{C}(\boldsymbol{x}) = d(c_3 - c_1)x_1x_3. \tag{17}$$

When $c_1 \neq c_3$ and $d \neq 0$, the Casimir power becomes non-zero. In other words, these 5D equations are not conservative in Casimir energy. The divergences of these systems are described as

$$\nabla V = \frac{\partial \dot{x}_1}{\partial x_1} + \frac{\partial \dot{x}_2}{\partial x_2} + \frac{\partial \dot{x}_3}{\partial x_3} + \frac{\partial \dot{x}_4}{\partial x_4} + \frac{\partial \dot{x}_5}{\partial x_5} = 0, \tag{18}$$

which implies that the Hamiltonian conservative hyperchaotic system preserves volume in phase space.

Setting the parameters as c_1=1, c_2 =2, c_3=6, c_4=4, c_5=9, d=1, k_1=1, k_2=1, k_3=1, and k_4=-1, and the initial conditions as (0.8, 0.1, 0.8, 0.8, 0.8), the system shows a hyperchaotic state. The phase diagrams are presented in Figure 1, and the Poincaré map on $x_3 = 0$ is exhibited in Figure 2. The Lyapunov exponents of this system are $[1.073, 0.024, 0, 0.052, -1.043]^T$. The Lyapunov dimension is

$$D_L = D_{KY} = j + \frac{\sum_{i=1}^{j} L_i}{|L_{j+1}|} = 5. \tag{19}$$

The Lyapunov dimension is the same as the number of variables and is an integer. This demonstrates that the system is a conservative hyperchaotic system. However, the Lyapunov dimension of dissipative chaotic systems is a fractional number.

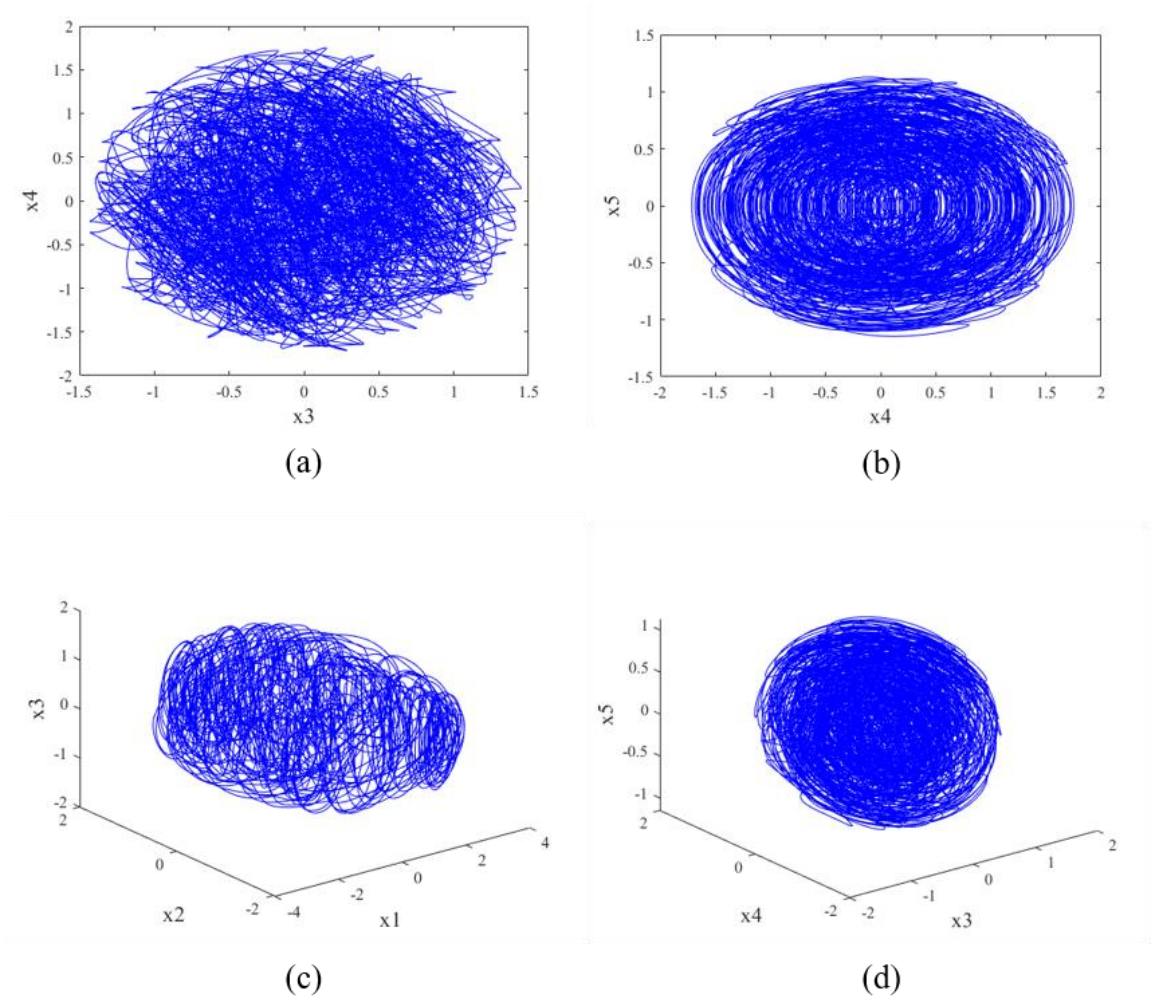

Figure 1. Phase diagrams of the Hamiltonian conservative hyperchaotic system: (a) x_3-x_4 phase diagram, (b) x_4-x_5 phase diagram, (c) x_1-x_2-x_3 3D phase diagram, (d) x_3-x_4-x_5 3D phase diagram.

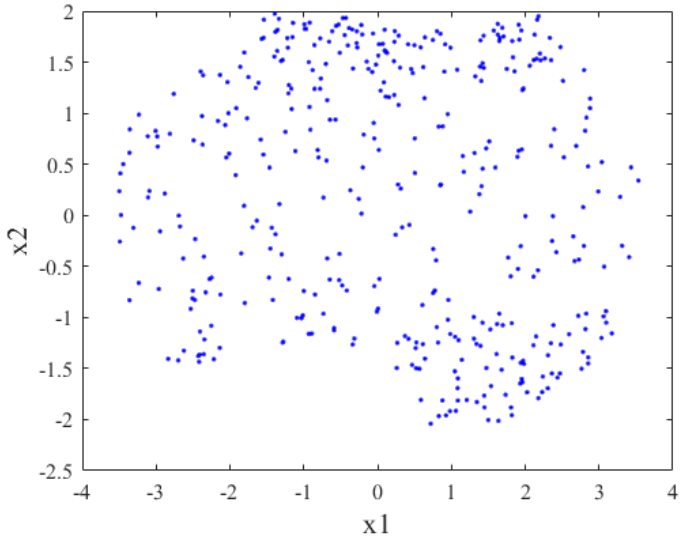

Figure 2. Poincaré map of the Hamiltonian conservative hyperchaotic system on $x_3 = 0$.

4. Analysis of the 5D novel Hamiltonian conservative hyperchaotic system

4.1. Equilibrium point analysis

By calculating, one obtains the equilibrium points of the system: $E_0(0, 0, 0, 0, 0)$, $E_1(0, p, 0, 0, 0)$, $E_2(0, 0, 0, q, 0)$ and $E_3(0, 0, 0, 0, r)$, where p, q, and $r \in R$. The system exhibits three equilibrium lines, indicating that this system possesses hidden dynamic behaviors and multistability. By computing $|\lambda I - J_{Ei}| = 0$, the corresponding eigenvalues and the equilibrium type can be obtained as shown in Table 1. Since the equilibrium of the system is either center or saddle, this conservative system lacks attractors and exclusively generates periodic, quasi-periodic, and hyperchaotic trajectories. The hyperchaotic trajectories are conservative hidden hyperchaotic trajectories.

Table 1. Equilibrium points and corresponding equilibrium type.

Equilibrium point	Eigenvalues	Equilibrium type
(0, 0, 0, 0, 0)	(0, 0, 0, $j\omega_1$, -$j\omega_1$)	Center
(0, p, 0, 0 ,0)	(0, σ_1, -σ_1, $j\omega_1$, -$j\omega_1$)	Saddle
(0, 0, 0, q ,0)	(0, σ_1, σ_2, σ_3+$j\omega_1$, σ_3−$j\omega_1$) (0, σ_1+$j\omega_1$, σ_1−$j\omega_1$, −σ_1+$j\omega_2$, −σ_1−$j\omega_2$)	Saddle
(0, 0, 0, 0 ,r)	(0, σ_1, σ_2, $\sigma_3 + j\omega_1$, $\sigma_3 - j\omega_1$) (0, σ_1+$j\omega_1$, σ_1−$j\omega_1$, −σ_1+$j\omega_2$, −σ_1−$j\omega_2$)	Saddle

4.2. Analyses by the theory of KAM perturbation

The theorem of KAM perturbation is a theory to analyze Hamiltonian chaotic systems [24]. We use the KAM perturbation theorem to analyze the proposed hyperchaotic system. Eq (15) can be written as

$$\dot{\boldsymbol{x}} = J(\boldsymbol{x})\nabla H(\boldsymbol{x}) + J'(\boldsymbol{x})\nabla H_1(\boldsymbol{x}), \tag{20}$$

where

$$J'(\boldsymbol{x}) = \begin{bmatrix} 0 & 0 & -d & 0 & 0 \\ 0 & 0 & 0 & 0 & 0 \\ d & 0 & 0 & 0 & 0 \\ 0 & 0 & 0 & 0 & 0 \\ 0 & 0 & 0 & 0 & 0 \end{bmatrix} \tag{21}$$

and

$$H_1(\boldsymbol{x}) = \frac{1}{2}(c_1 x_1^2 + c_3 x_3^2). \tag{22}$$

Therefore, $H_1(\mathbf{x})$ can be considered as a perturbation term. The perturbed Hamiltonian system may produce chaos. We can use the Casimir power to analyze it. Figure 3 shows that the zero line is the center of oscillation for the Casimir power. The Casimir power oscillation illustrates that the perturbed Hamiltonian system generates chaos.

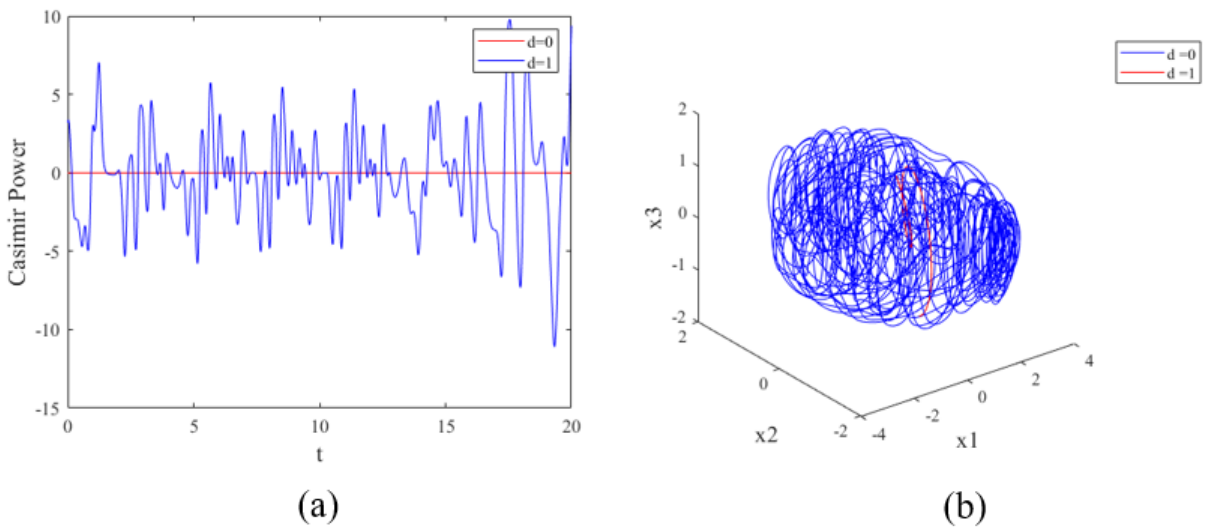

Figure 3. Casimir Power and phase diagram with different d: (a)Time-waveform of Casimir power oscillation, (b) x_1-x_2-x_3 phase diagram.

4.3. Influences of system parameters

Herein, the influence of the parameter k_4 on the system is investigated, and the Lyapunov exponent spectrum and the bifurcation diagram concerning the parameter k_4 are drawn, where the parameters are c_1=1, c_2 =2, c_3=6, c_4=4, c_5=9, d=1, k_1=1, k_2=1 and k_3=1, and the initial conditions are (0.8,0.1,0.8,0.8,0.8). As shown in Figure 4, as the parameter k_4 varies from -1 to 1, the amplitude does not change significantly, and the Lyapunov exponent only shows slight variations, remaining positive throughout. Therefore, the system is suitable for encryption.

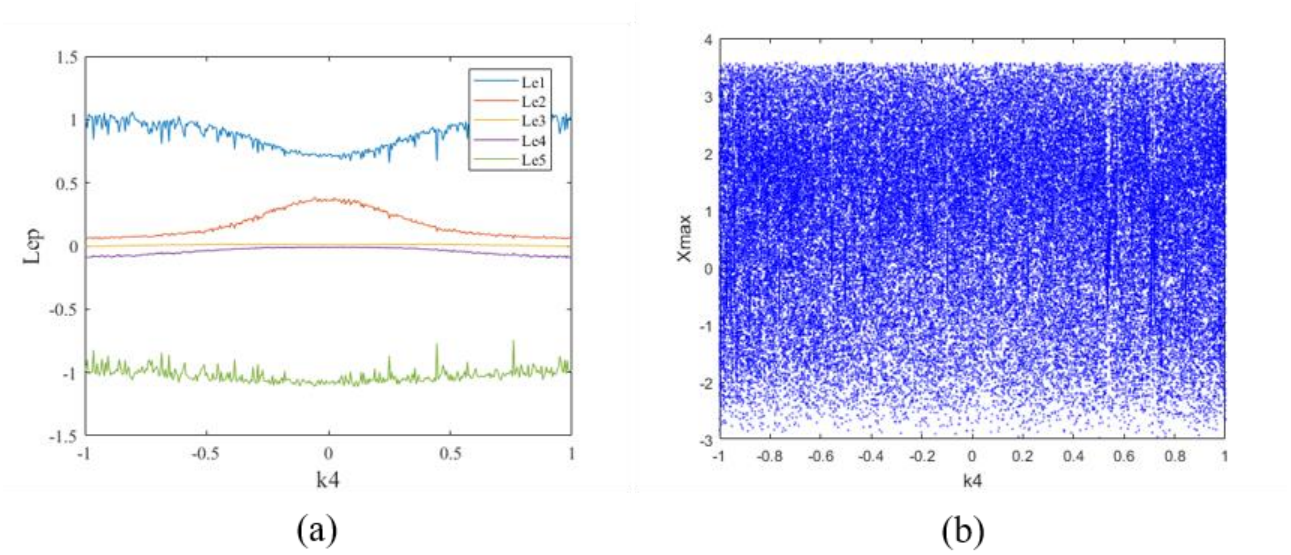

Figure 4. Lyapunov exponent spectrum (a) and bifurcation diagram (b) versus the parameter k_4.

In addition, the impact of the parameter c_5 on the system is also analyzed. Figure 5(a) shows that two largest Lyapunov exponents are more than zero in the interval [0.5, 3000]. The bifurcation diagram in Figure 5 shows that the amplitude of variable x increases with the parameter c_5 increasing. Therefore, the system has a wide parameter range and is amplitude-controllable. Specifically, when the parameter c_5 takes the values of 10, 100, and 1000, the time-domain diagrams of x_3 and the phase diagram of x_3-x_4 are displayed in Figure 6. It is evident that the amplitude of the system increases with the parameter c_5.

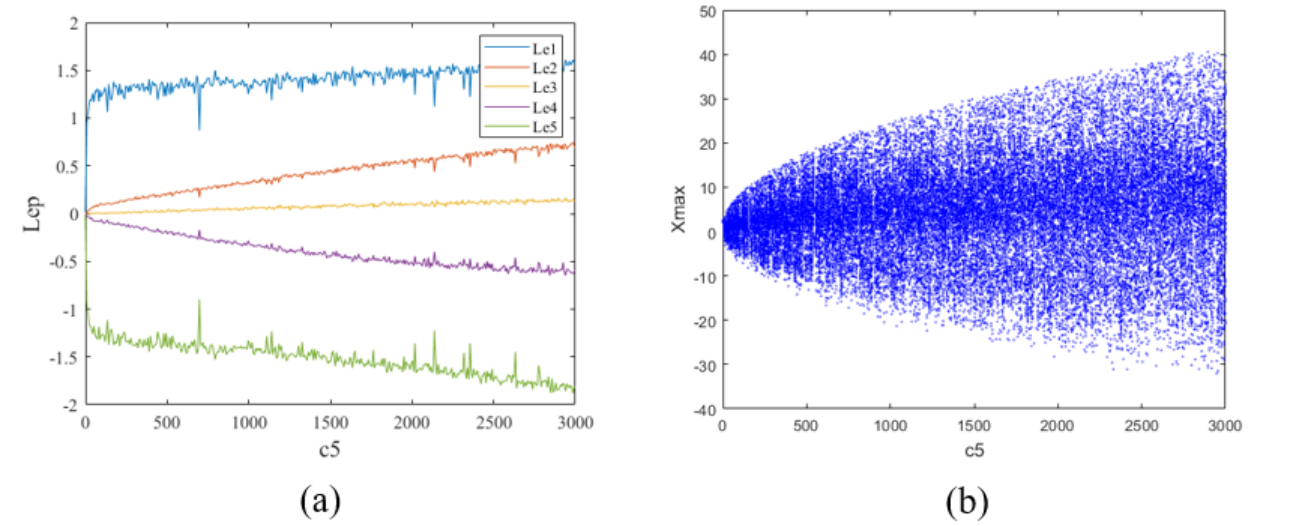

Figure 5. Lyapunov exponent spectrum (a) and bifurcation diagram (b) versus the parameter c_5.

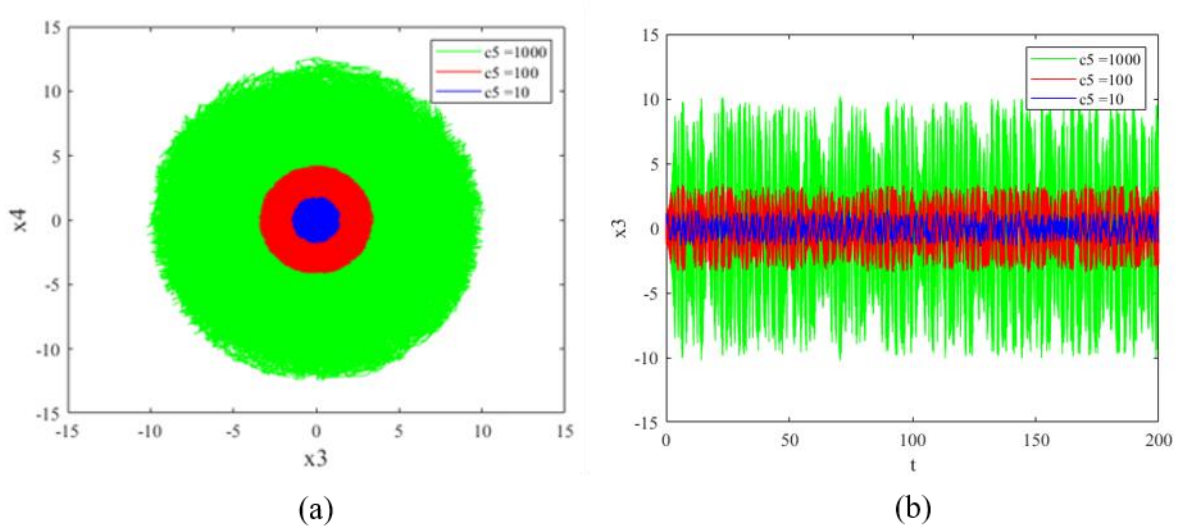

Figure 6. Phase diagram and time-waveform against c_5: (a) phase diagrams, (b) time-waveforms with c_5=10, 100, and 1000.

4.4. Influences of initial conditions

This section analyzes the impact of initial values. Under the parameters of c_1=1, c_2 =2, c_3=6, c_4=4, c_5=9, d=1, k_1=1, k_2=1, k_3=1, and k_4=-1, the Lyapunov exponent spectrum and the bifurcation diagram concerning the initial value $x_1(0)$ are displayed in Figure 7, where the other initial value $x_i(0)$=0.01. Figure 7(b) demonstrates that the amplitude of variable x increases with the initial value $x_1(0)$ increasing, indicating that the system exhibits multistability and initial-condition amplitude control. Multistability refers to the phenomenon that a chaotic system presents multiple phase trajectories of topological structures or different positions with the change of initial conditions without changing the system parameters. Multistability includes homogeneous multistability and heterogeneous multistability. If the coexistence flows have the same shape but differ in positions, frequencies, or amplitudes, the multistability is homogeneous multistability. Otherwise, it is heterogeneous multistability. Specifically, when the initial value $x_1(0)$ is taken as 0.3, 0.6, and 1, the time-domain diagrams of x_3 and the phase diagrams of x_3-x_4 are shown in Figure 8. From Figure 8(a), it can be observed that the coexistence flows have the same shape and different amplitude. Hence, this multistability is homogeneous multistability. Moreover, with the initial value $x_1(0)$ increasing, the amplitude of the system increases, which demonstrates initial-condition amplitude control. Compared with the 5D hyperjerk-type hyperchaotic system in Reference [25], the conservative hyperchaotic system has initial-condition amplitude control.

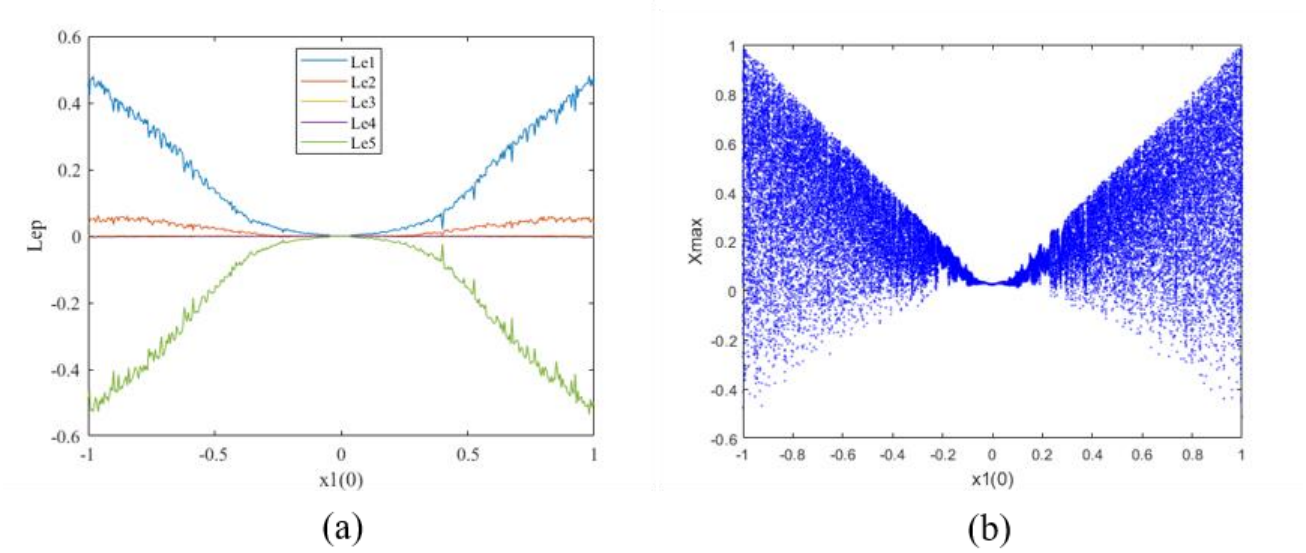

Figure 7. Lyapunov exponent spectrum (a) and bifurcation diagram (b) versus the parameter $x_1(0)$.

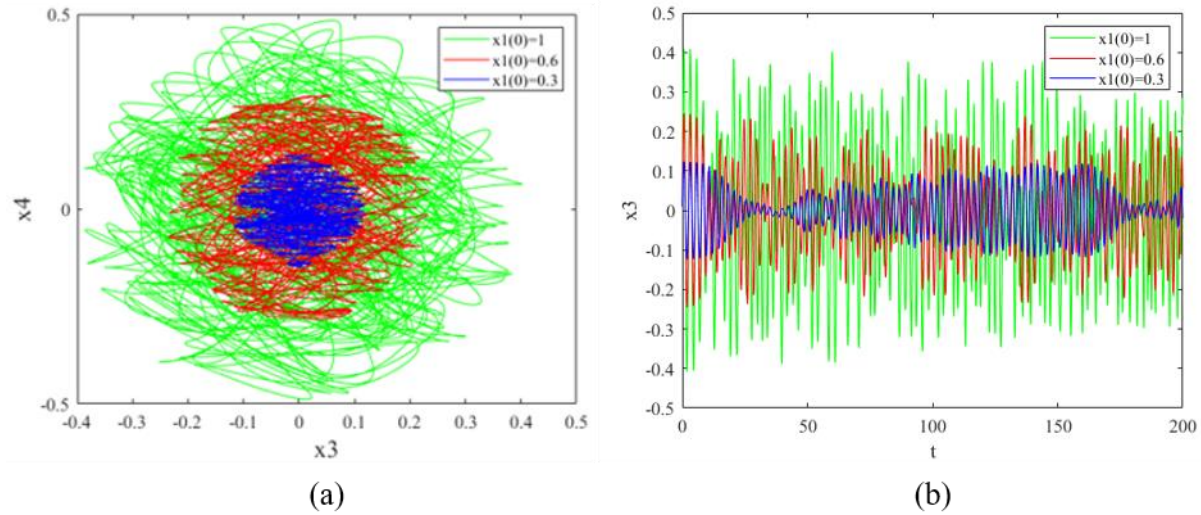

Figure 8. Phase diagram and time-waveform against $x_1(0)$: (a) phase diagrams, (b) time-waveforms with $x_1(0)$=1, 0.6, and 0.3.

The multistability of the system is related to the Hamiltonian. Choosing the parameters as c_1=1, c_2 =2, c_3=6, c_4=4, c_5=9, d=1, k_1=1, k_2=1, k_3=1, and k_4=-1,the Hamiltonian distribution diagram is plotted in Figure 9. The vertical axis and color bars represent the values of Hamiltonian energy. The initial conditions of Figure 9(a) are ($x_1(0)$, 0.01, 0.01, 0.01, $x_5(0)$), while the ones of Figure 9(b) are (0.01, 0.01, x_3 (0), x_4 (0), 0.01). The Hamiltonian of Figure 9(a) and 9(b) are respectively expressed as:

$$H = \frac{1}{2}(x_1^2 + 9x_5^2 + 0.0012). \tag{23}$$

$$H = \frac{1}{2}(6x_3^2 + 4x_4^2 + 0.0012). \tag{24}$$

As shown by the contour lines at the bottom of Figure 9, the Hamiltonian forms a circular distribution. Generally speaking, orange corresponds to strong chaotic orbits, and dark blue corresponds to quasi-periodic or weak chaos. Therefore, the energy distribution of the double initial values intuitively reflects the changing trend of dynamic behavior.

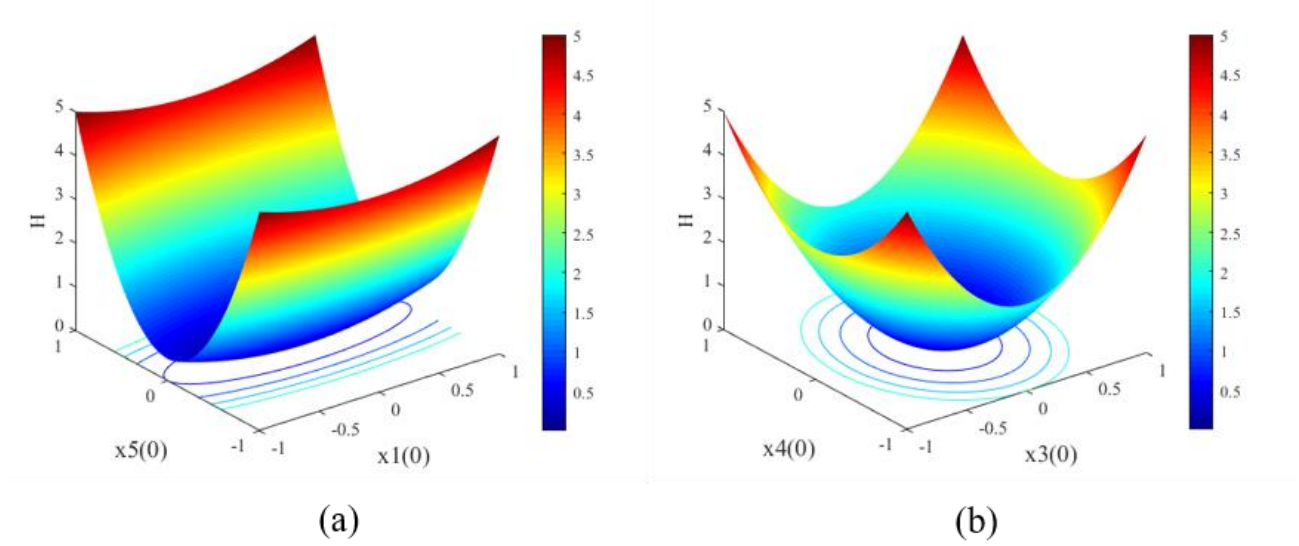

Figure 9. Hamiltonian distribution diagram in (a) $x_1(0)$–$x_5(0)$ plane and (b) $x_3(0)$–$x_4(0)$ plane.

Variations in the Hamiltonian lead to both homogeneous and heterogeneous multistability in this system. The multistability of the system is demonstrated in Figure 10, which shows the coexistence of quasiperiodic states, the coexistence of quasiperiodic and hyperchaotic states, and the coexistence of hyperchaotic states. Figure 10(a) and 10(c) are homogeneous multistability, while Figure 10(b) is heterogeneous multistability. Due to the multistability of the system, taking the initial value of the system as the key will enhance the sensitivity of the key and strengthen the resistance to attacks. With a computational accuracy of 10^{-10}, the key space is $10^{10}\times10^{10}\times10^{10}\times10^{10}\times10^{10}=10^{50}\approx2^{161}>2^{100}$, implying that the key space is large enough to withstand a brute-force attack.

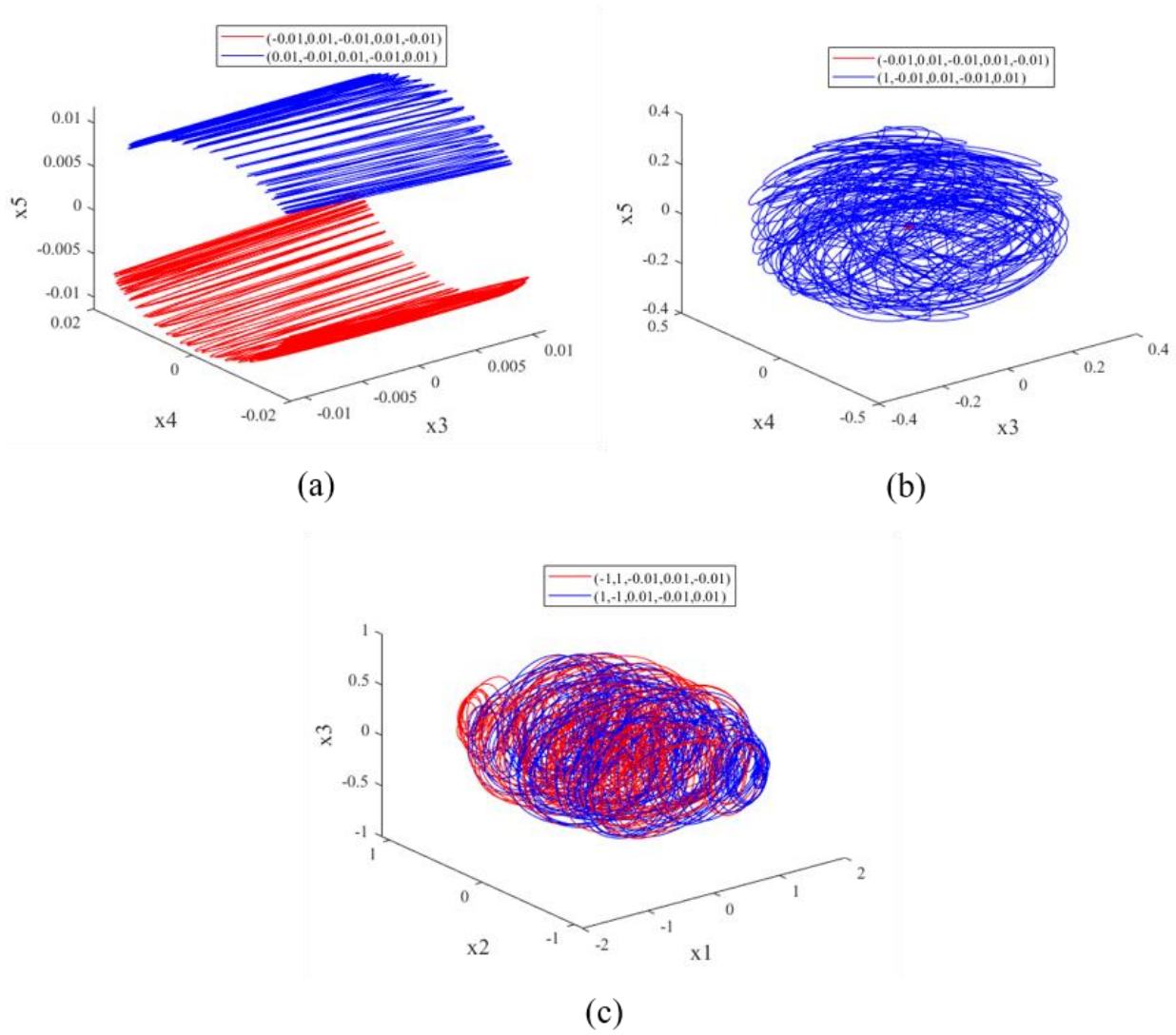

Figure 10. Orbit coexistence: (a) coexistence of quasiperiodic states, (b) coexistence of quasiperiodic and hyperchaotic states, (c) coexistence of hyperchaotic states.

4.5. Transient quasi-period

Transient quasi-period refers to the situation where a trajectory begins as a quasi-periodic trajectory and, after a period of time, suddenly transforms into a chaotic or hyperchaotic orbit. When the parameters are set as c_1=2, c_2 =2, c_3=5, c_4=4, c_5=9, d=1, k_1=1, k_2=1, k_3=1, and k_4=-1, and the initial conditions are (0.1455,0.1455,0.1455,0.1455,0.1455), the conservative system appears transient quasi-period as shown in Figure 11. Figure 11(a) demonstrates that the trajectory enters a hyperchaotic orbit from a quasi-periodic orbit when t=84.01s, and after that the system is in a hyperchaotic state. In Figure 11(b), the phase diagram of transient quasi-periodic state is represented in red, while that of hyperchaotic state is represented in blue.

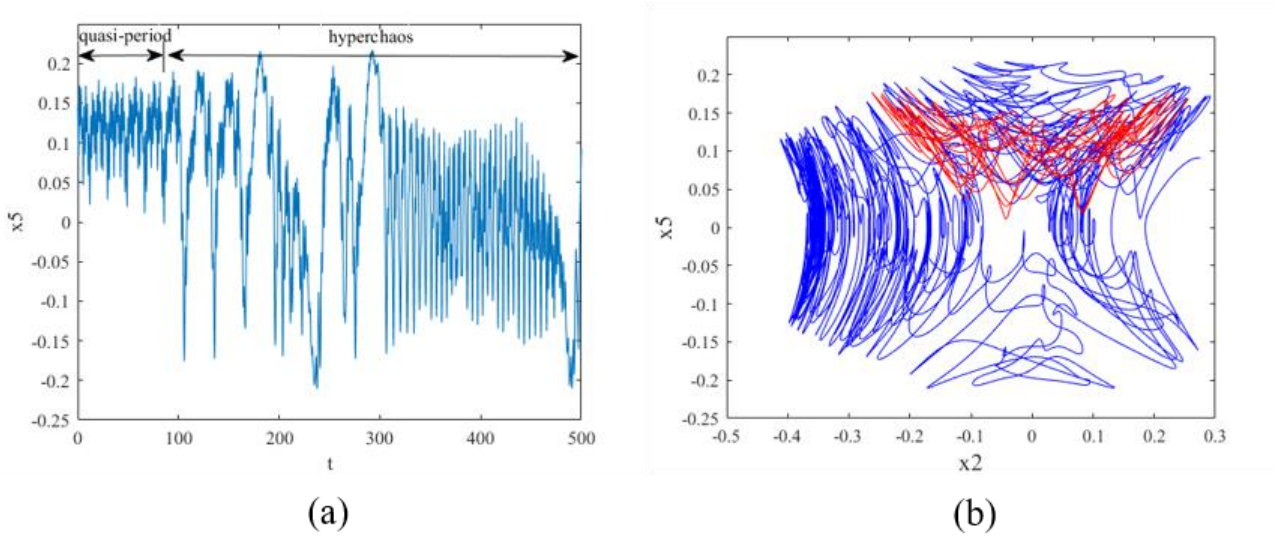

Figure 11. Transient quasi-period of the conservative system: (a) time-domain waveform and (b) x_2-x_5 phase diagram.

5. NIST test

NIST [26, 27] provides 15 test items for evaluating the statistical characteristics of random or pseudo-random sequences. A P-value is given at each test to determine if the sequence is random. Three requirements must be met by the test results in accordance with the NIST standard:

(1) The significance level $\alpha = 0.01$ cannot be lowered by any P-value, and P-value_T cannot be less than 0.0001.

(2) The confidence interval calculated by $\hat{p} \pm \sqrt{\hat{p}(1-\hat{p})/m}$ must contain an adequate proportion, where it is $\hat{p} = 1 - \alpha$. The proportion should fall between 0.9602 and 1.0198 if $m = 100$.

(3) The distribution of P-value must conform with uniformity.

In the test, we assign the parameters to c_1=1, c_2 =2, c_3=6, c_4=4, c_5=9, d=1, k_1=1, k_2=1, k_3=1, k_4=-1, and the initial conditions to (0.8, 0.1, 0.8, 0.8, 0.8). Subsequently, the hyperchaotic sequences produced by the proposed system are transformed into binary format and segmented into 100 groups for the NIST statistical test. The NIST SP800-22 Statistical Test Suite is utilized to assess the randomness of the sequences. The test results are presented in Table 2, where all test items have P-values above the significance level and the corresponding proportions fall within the confidence interval. The smallest proportion of the proposed Hamiltonian conservative hyperchaotic system is 0.98, and is greater than the one of the Hamiltonian conservative chaotic system in Reference [16], thus being more suitable as a random sequence generator. Furthermore, the Non-overlapping Template Matching Test uses an m= 9 bit template to test all 148 NIST predefined aperiodic patterns. The histogram of the non-overlapping template (as shown in Figure 12) indicates that the distribution of P-values exhibits excellent uniformity. Moreover, all tests of TestU01 are passed by applying the method in Reference [26]. Consequently, the pseudo-random sequences meet the test requirements effectively. If the generated pseudo-random sequence is used as the key and combined with homomorphic encryption technology, multiple encryption method, sequence rearrangement method and other methods, the pseudo-random sequence can be used in encryption protocols or secure data

transmission systems.

Table 2. NIST test results.

No.	Statistical test	P-value	P-value$_T$	Proportion
1	Frequency	0.732351	0.275709	1.00
2	Block frequency	0.569989	0.911413	1.00
3	Cumulative sums	0.586832	0.213309	0.99
4	Runs	0.253503	0.213309	1.00
5	Longest run	0.949671	0.637119	1.00
6	Rank	0.613152	0.637119	1.00
7	FFT	0.192547	0.971699	1.00
8	Non-overlapping template	0.361381	0.485569	0.99
9	Overlapping template	0.026274	0.595549	0.98
10	Universal	0.154142	0.534146	1.00
11	Approximate entropy	0.679859	0.657933	1.00
12	Random excursions	0.454725	0.911413	1.00
13	Random excursions variant	0.585896	0.327854	1.00
14	Serial(1st)	0.371761	0.181557	0.99
15	Linear complexity	0.533699	0.798139	0.99

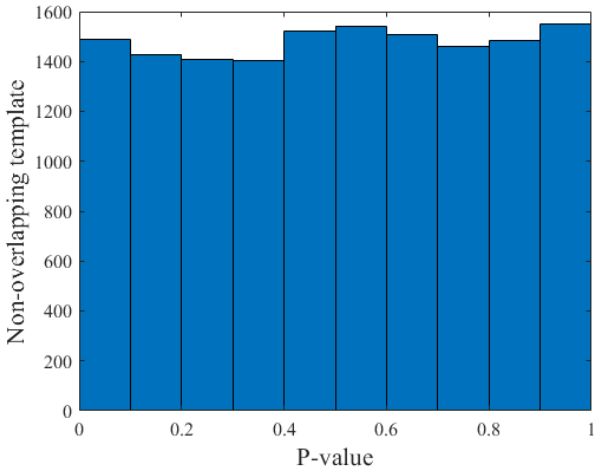

Figure 12. P-value histogram of the non-overlapping template.

6. Circuit realization

6.1. Analog circuit implementation

Since analog circuits are the most direct and realistic manifestation of chaos theory in the physical world, the analog circuits commonly serve as implementation platforms for chaotic or hyperchaotic systems. In this section, an analog circuit is designed to validate the physical feasibility of the Hamiltonian conservative hyperchaotic system. First, by substituting c_1=1, c_2 =2, c_3=6, c_4=4, c_5=9, d=1, k_1=1, k_2=1, k_3=1, and k_4=-1 into Eq (15), the equation becomes

$$\begin{cases} \dot{x}_1 = 5x_4x_5 - 6x_3, \\ \dot{x}_2 = 5x_4x_5 - 3x_3x_5, \\ \dot{x}_3 = 5x_4x_5 + 7x_2x_5 + x_1, \\ \dot{x}_4 = -8x_1x_5 - 7x_2x_5 - 3x_3x_5, \\ \dot{x}_5 = 3x_1x_4 + 2x_2x_4 - 2x_3x_4 - 4x_2x_3. \end{cases} \tag{25}$$

Then, we design the equivalent circuit on the Multisim platform. The circuit schematic diagram is demonstrated in Figure 13, where the time scaling factor is chosen as k=10, i.e., t=10τ. The circuit includes analog resistors, capacitors, operational amplifiers, and multipliers, whose parameters are shown in Figure 13. Finally, after we run the circuit, the phase portraits of the system are recorded by the oscilloscope. Figure 14 illustrates that the x_3-x_4 and x_4-x_5 phase diagrams agree well with those of the Matlab software. Chaotic analog circuits can generate real chaotic signals in real time and at high speed, and can be applied in the fields such as secure communication, radar and detection.

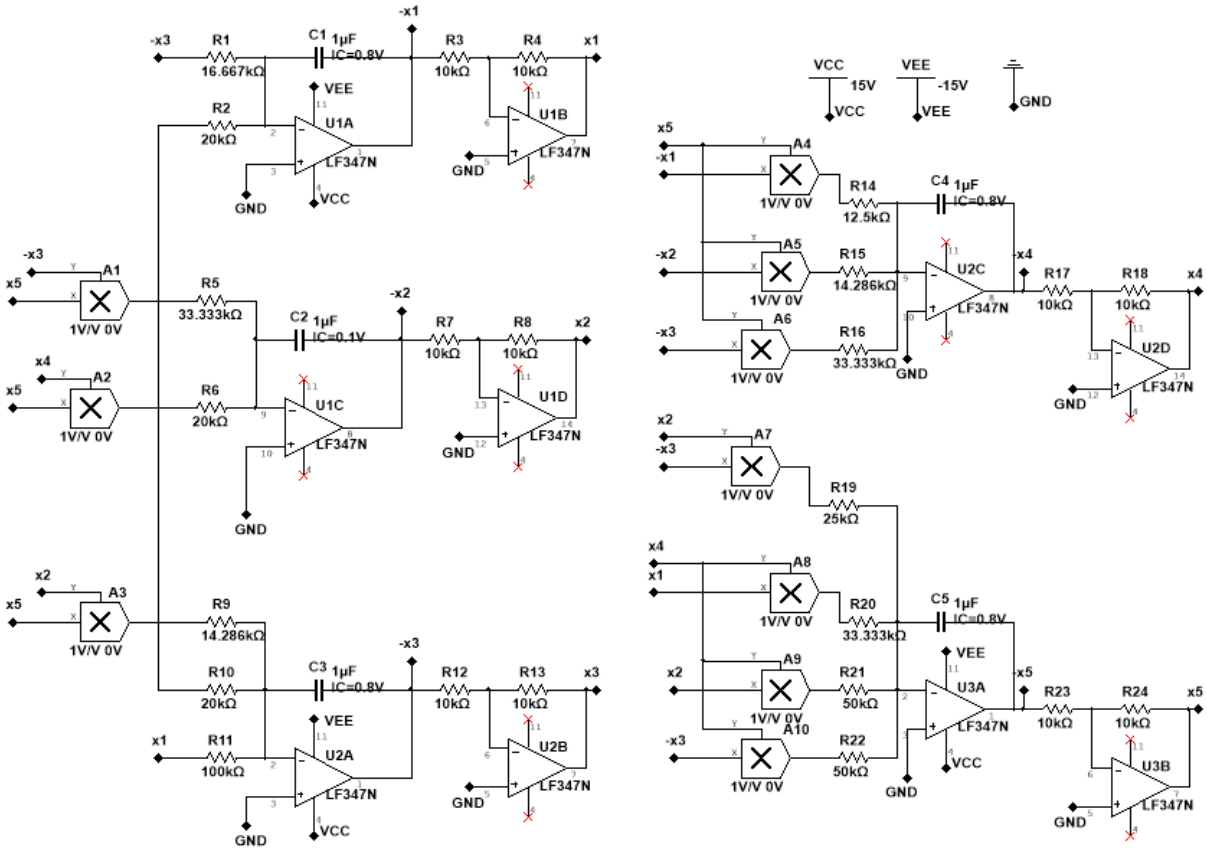

Figure 13. Circuit schematic of the Hamiltonian conservative hyperchaotic system.

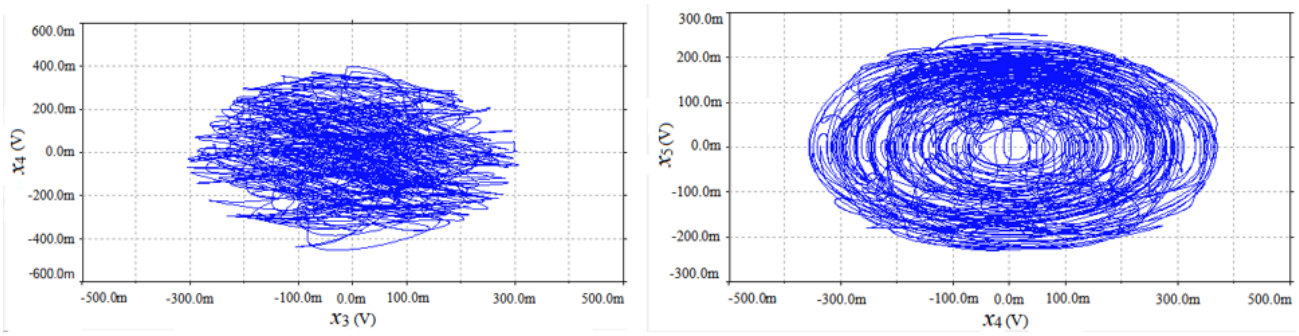

Figure 14. Simulation results of the conservative system in (a) x_3-x_4 plane and (b) x_4-x_5 plane.

6.2. Hardware implementation of the STM32 platform

Hardware implementation plays a crucial role in hyperchaotic system investigation.Compared with FPGA, raspberry Pi, arduino and so on, STM32 has the advantages of easy implementation, low power consumption and low cost. We choose STM32F407EVT6 as the signal processing chip. Then the Runge-Kutta algorithm is employed to discretize the mathematical system, and the C language is used for programming. When the parameters are assigned as c_1=1, c_2 =2, c_3=6, c_4=4, c_5=9, d=1, k_1=1, k_2=1, k_3=1, and k_4=-1, and the initial conditions chosen to be (0.8, 0.1, 0.8, 0.8, 0.8), the results shown in Figure 15 are observed by the SDS-2000X Plus oscilloscope. Figure 15(b) coincides with Figure 1(a) of the Matlab simulation results, implying the physical realizability. Based on the STM32 chaotic system, chaotic key streams can be generated for data encryption of Internet of Things (IoT) devices. The program design of STM occupies 1M of memory. Due to the use of 12-bit DAC output, the hardware-vs-simulation error is approximately 2.44×10^{-4}. Recently, the design of chaotic systems uses CMOS integrated circuit technology to design, which has low power consumption. Next, such circuits will be designed using CMOS technology.

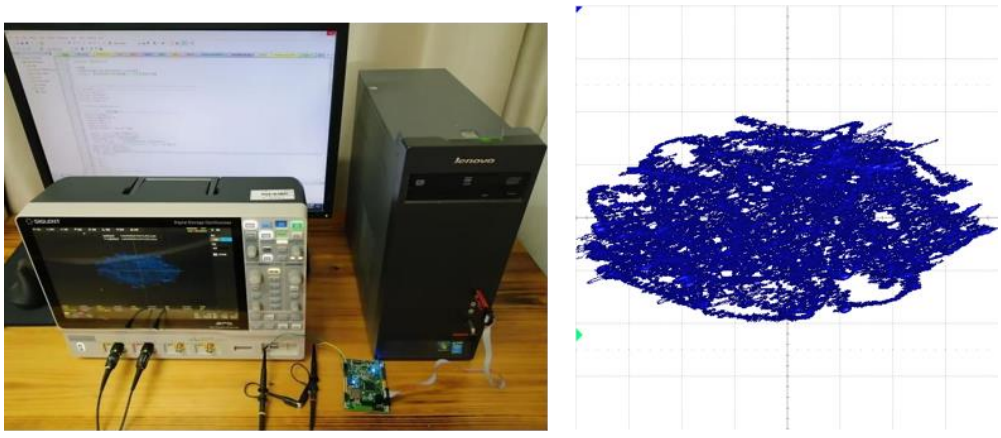

Figure 15. Experimental results of the conservative system: (a) Experimental setup of STM32, (b) x_3-x_4 phase diagrams by STM32.

7. Comparative analysis

To visually illustrate that the system construction method, dynamical behaviors and implementation differ from the existing results, Table 3 lists the comparison results with the existing conservative chaotic systems. Reference [12] constructed a 5D conservative memristive hyperchaotic system by introducing a memristor, which had complicated dynamic behaviors, such as multistability, ultra-wide range and transient quasi-period, but is a Non-HCCS. The others were designed by using the generalized Euler equation, and belonged to the HCCS. It can be seen that References [17–20] obtain 5D systems by coupling two generalized Euler sub-bodies with one common axis. Our method is to construct a 5D Hamiltonian conservative hyperchaotic system by coupling four sub-bodies with the four parameters, which differs from References [17–20]. In Reference [16], a 4D Hamiltonian conservative chaotic system is built via the same method as ours. However, the Hamiltonian conservative system is chaotic, and its dynamic behaviors only has transient quasi-period and multistability. Our designed system exhibits more complicated nonlinear behaviors than the other, which has amplitude control, multistability, transient quasi-period, and a wide constant range. Moreover, comparing with other platforms, the STM32 platform to hardware implementation possesses the advantages of easy implementation, low power consumption and low cost. Therefore, the proposed approach to construct and implement Hamiltonian conservative hyperchaotic systems has effectively expanded the theoretical basis of available Hamiltonian conservative chaotic or hyperchaotic systems.

Table 3. Comparative results.

System	Type	Construction method	Dimension	Complicated nonlinear characteristics	Circuit realization
Reference 12	Non-HCCS	Introducing a memristor into a 4D CCS	5D	Multistability, ultra-wide range and transient quasi-period	--
Reference 16	HCCS	Coupling four sub-bodies with four parameters	4D	Transient quasi-period and multistability	FPGA
Reference 17	HCCS	Coupling two sub-bodies with one common axis	5D	Multistability	FPGA
Reference 18	HCCS	Coupling two sub-bodies with one common axis	5D	Wide parameter range	Analog Circuit
Reference 19	HCCS	Coupling two sub-bodies with one common axis	5D	Multistability, wide range and transient transition	DSP

Continued on next page

System	Type	Construction method	Dimension	Complicated nonlinear characteristics	Circuit realization
Reference 20	HCCS	Coupling two sub-bodies with one common axis	5D	Multistability	Analog Circuit, DSP
Ours	HCCS	Coupling four sub-bodies with four parameters	5D	Amplitude control, multistability, transient quasi-period, and a wide constant range	Analog Circuit, STM32

8. Conclusions

This paper presents a 5D Euler equation constructed from four 5D Euler subsystems, which maintains the conservation of both Hamiltonian and Casimir energy. A 5D Hamiltonian conservative hyperchaotic system is designed by violating the conservation of Casimir energy. This hyperchaotic system possesses nonlinear properties such as a wide range of constants, multistability, transient quasi-period, and amplitude control. These nonlinear characteristics make the system suitable for secure communication. The NIST test demonstrates that the pseudo-random sequences produced by the system exhibit good randomness. Lastly, the feasibility of the system is proven using simulation circuits and the STM32 platform. This system has good pseudo-random characteristics, indicating that it has potential applications in the field of encryption. The work effectively expanded the theoretical basis of Hamiltonian conservative hyperchaotic systems. Moreover, we can change the coupling parameters to build more 5D Hamiltonian conservative hyperchaotic systems.

Author contributions

Zhitao Xu: Writing—original draft, Software, Visualization. Birong Xu: Methodology, Writing—review & editing, Software, Hardware, Validation. All authors have read and approved the final version of the manuscript for publication.

Use of AI tools declaration

The authors declare they have not used Artificial Intelligence (AI) tools in the creation of this article.

Acknowledgments

This work was supported in part by the Natural Science Foundations of Fujian Province (Grant No. 2020J01395, 2024J01320).

Conflict of interest

The authors declare there is no conflict of interest.

References

1. G. Li, X. Xu, H. Zhong, A image encryption algorithm based on coexisting multi-attractors in a spherical chaotic system, *Multimed Tools Appl.*, **81** (2022), 32005–32031. https://doi.org/10.1007/s11042-022-12853-9
2. N. F. Karagiorgos, S. G. Stavrinides, C. de Benito, S. Nikolaidis, R. Picos, Unconventional security for IoT: Hardware and software implementation of a digital Chaotic encrypted communication scheme, *IEEE Internet Things J.*, **11** (2024), 19914–19925. https://doi.org/10.1109/JIOT.2024.3371091
3. T. Abdeljawad, M. Sher, K. Shah, M. Sarwar, I. Amacha, M. Alqudah, et al., Analysis of a class of fractal hybrid fractional differential equation with application to a biological model, *Sci. Rep.*, **14** (2024), 18937. https://doi.org/10.1038/s41598-024-67158-8
4. K. Morijiri, K. Takehana, T. Mihana, K. Kanno, M. Naruse, A. Uchida, Parallel photonic accelerator for decision making using optical spatiotemporal chaos, *Optica*, **10** (2023), 339–348. https://doi.org/10.1364/OPTICA.477433
5. X. Wu, Y. Sun, Y. Wang, Y. Chen, Passive chaos suppression for the planar slider-crank mechanism with a clearance joint by attached vibro-impact oscillator, *Mech. Mach. Theory*, **174** (2022), 104882. https://doi.org/10.1016/j.mechmachtheory.2022.104882
6. Q. Wang, Y. Yang, X. Zhang, Weak signal detection based on Mathieu-Duffing oscillator with time-delay feedback and multiplicative noise, *Chaos Soliton. Fract.*, **137** (2020), 109832. https://doi.org/10.1016/j.chaos.2020.109832
7. M. D. Vijayakumar, H. Natiq, M. I. T. Meli, G. D. Leutcho, Z. T. Njitacke, Hamiltonian energy computation of a novel memristive mega-stable oscillator (MMO) with dissipative, conservative and repelled dynamics, *Chaos Soliton. Fract.*, **155** (2022), 111765. https://doi.org/10.1016/j.chaos.2021.111765
8. S. Wu, G. Li, W. Xu, X. Xu, H. Zhong, Modelling and dynamic analysis of a novel seven-dimensional Hamilton conservative hyperchaotic systems with wide range of parameter, *Phys. Scr.*, **98** (2023), 055218. https://doi.org/10.1088/1402-4896/accd2c
9. S. Cang, Y. Li, W. Xue, Z. Wang, Z. Chen, Conservative chaos and invariant tori in the modified Sprott A system, *Nonlinear Dyn.*, **99** (2020), 1699–1708. https://doi.org/10.1007/s11071-019-05385-9
10. E. Dong, M. Yuan, S. Du, Z. Chen, A new class of Hamiltonian conservative chaotic systems with multistability and design of pseudo-random number generator, *Appl. Math. Model.*, **73** (2019), 40–71. https://doi.org/10.1016/j.apm.2019.03.037
11. S. Cang, A. Wu, Z. Wang, Z. Chen, Four-dimensional autonomous dynamical systems with conservative flows: two-case study, *Nonlinear Dyn.*, **89** (2017), 2495–2508. https://doi.org/10.1007/s11071-017-3599-6

12. F. Yu, B. Tan, T. He, S. He, Y. Huang, S. Cai, et al., A wide-range adjustable conservative memristive hyperchaotic system with transient quasi-periodic characteristics and encryption application, *Mathematics*, **13** (2025), 726. https://doi.org/10.3390/math13050726
13. G. Qi, Modelings and mechanism analysis underlying both the 4D Euler equations and Hamiltonian conservative chaotic systems, *Nonlinear Dyn.*, **95** (2019), 2063–2077. https://doi.org/10.1007/s11071-018-4676-1
14. G. Qi, J. Hu, Z. Wang, Modeling of a Hamiltonian conservative chaotic system and its mechanism routes from periodic to quasiperiodic, chaos and strong chaos, *Appl. Math. Model.*, **78** (2020), 350–365. https://doi.org/10.1016/j.apm.2019.08.023
15. G. Qi, J. Hu, Modelling of both energy and volume conservative chaotic systems and their mechanism analyses, *Commun. Nonlinear Sci.*, **84** (2020), 105171. https://doi.org/10.1016/j.cnsns.2020.105171
16. F. Yu, Y. Yuan, C. Wu, W. Yao, C. Xu, S. Cai, et al., Modeling and hardware implementation of a class of Hamiltonian conservative chaotic systems with transient quasi-period and multistability, *Nonlinear Dyn.*, **112** (2024), 2331–2347. https://doi.org/10.1007/s11071-023-09148-5
17. E. Dong, X. Jiao, S. Du, Z. Chen, G. Qi, Modeling, synchronization, and FPGA implementation of Hamiltonian conservative hyperchaos, *Complexity*, **2020** (2020), 4627597. https://doi.org/10.1155/2020/4627597
18. Z. Zhang, L. Huang, J. Xiang, S. Liu, Dynamic study of a new five-dimensional conservative hyperchaotic system with wide parameter range, *Acta Phys. Sin.*, **70** (2021), 230501. https://doi.org/10.7498/aps.70.20210592
19. Z. Zhang, L. Huang, A new 5D Hamiltonian conservative hyperchaotic system with four center type equilibrium points, wide range and coexisting hyperchaotic orbits, *Nonlinear Dyn.*, **108** (2022), 637–652. https://doi.org/10.1007/s11071-021-07197-2
20. L. Huang, Y. Ma, C. Li, Characteristic analysis of 5D symmetric Hamiltonian conservative hyperchaotic system with hidden multiple stability, *Chin. Phys. B*, **33** (2024), 010503. https://doi.org/10.1088/1674-1056/acf9e7
21. X. Ning, Q. Dong, S. Zhou, Q. Zhang, N. K. Kasabov, Construction of new 5D Hamiltonian conservative hyperchaotic system and its application in image encryption, *Nonlinear Dyn.*, **111** (2023), 20425–20446. https://doi.org/10.1007/s11071-023-08866-0
22. G. D. Leutcho, G. Gandubert, L. Woodward, F. Blanchard, Electric-field-biased control of irregular oscillations via multistability in a nonlinear terahertz meta-atom, *Chaos Soliton. Fract.*, **198** (2025), 116586. https://doi.org/10.1016/j.chaos.2025.116586
23. S. Ding, H. Lin, X. Deng, W. Yao, J. Jin, A hidden multiwing memristive neural network and its application in remote sensing data security, *Expert Syst. Appl.*, **277** (2025), 127168. https://doi.org/10.1016/j.eswa.2025.127168
24. M. V. Shamolin, Classification of complete integrability cases in four-dimensional symmetric rigid-body dynamics in a nonconservative field, *J. Math. Sci.*, **165** (2010), 743–754. https://doi.org/10.1007/s10958-010-9838-8
25. G. Vivekanandhan, J. C. Chedjou, K. Jacques, K. Rajagopal, A unique self-driven 5D hyperjerk circuit with hyperbolic sine function: hyperchaos with three positive exponents, complex transient behavior and coexisting attractors, *Chaos Soliton. Fract.*, **186** (2024), 115276. https://doi.org/10.1016/j.chaos.2024.115276

26. A. Rukhin, J. Soto, J. Nechvatal, M. Smid, E. Barker, S. Leigh, et al., *A statistical test suite for random and pseudorandom number generators for cryptographic applications*, 2010.
27. L. G. D. L. Fraga, J. D. Rodríguez-Muñoz, E. Tlelo-Cuautle, *Random number generators: Verilog description, hardware implementation and applications*, Cham: Springer, 2025. https://doi.org/10.1007/978-3-031-82865-2

AIMS Press